Joint Special Interest Group meeting between euspen and ASPE
Advancing Precision in Additive Manufacturing
Inspire AG, St. Gallen, Switzerland 2021
www.euspen.eu

Surface topography process signatures in nickel superalloy 625 additive manufacturing

J.C. Fox(2), A. Allen(1), B. Mullany (1), E. Morse(1), R.A. Isaacs (3), M. Lata(1), A. Sood (1), and C. Evans (1,2)

[1] *University of North Carolina at Charlotte,* [2] *National Institute of Standards and Technology,* [3] *Zeiss*

cevans52@uncc.edu

Abstract

Prior analyses of surface measurements performed – by several groups – on laser powder bed fused metals have tended to use ISO standard short wavelength filters and focus on weld tracks, "chevrons" (melt pool wake), and particles. This work, utilizing two sets of nickel superalloy 625 samples fabricated in an EOS M290 three years apart, extends the palette of features analyzed. In addition to the previously identified features, coherence scanning interferometer measurements reveal fine dendritic structures with a base periodicity of order 1 μm and long-range order up to 100 μm. Localized areas of radial primary dendrites with orthogonal secondary dendrites are also observed. Additional observations include areas of disordered fine structure, fine particles, and localized thin films, presumably from the plume of condensing metal. The composition of these features is varied, both locally and across the extent of the samples.

Laser Powder Bed Fusion, Nickel Superalloy, Surface structure, Microstructure

1. Introduction

Laser powder bed fusion (LPBF) is one popular process for additive manufacturing (AM) of a range of metals, including superalloys such as nickel superalloy 625 (IN625) discussed here. Surface topography is widely used as one acceptance criterion in conventional manufacturing and as a process signature for process optimization and control. Top surfaces in LPBF have surface topographic features with amplitudes and spatial wavelengths greater and more diverse than in conventional machining that challenge conventional geometric metrology [1] and are poorly described by commonly used surface measurement parameters.

Prior analyses of surface measurements – performed by several groups – on laser powder bed fused metals have tended to focus on weld tracks, "chevrons" (melt pool wake), particles, undercuts, and cracks, as reviewed in [2] and cited references [1,3,4]. Here we report on additional textures and features with lateral scales varying from a 100 μm scale down to tens of nm on LPBF IN625.

2. Experimental methods

Two sets of samples were built in the progression of this study. The first is described in detail in Reese *et al.* [5]. The second set (12 samples) was fabricated in 2020 with integrated coordinate systems that allow the location of features measured with a variety of tools. The samples were built in IN625 using a commercially available EOS M290 system. Vendor recommended process parameters were used for the part, except the upskin (e.g., region near the upward facing surfaces) where parameters are varied to improve surface finish was turned off, maintaining interior characteristics of the build at the top surface for examination.

The data from sample 9 in the 2020 build is analyzed in this work (see Figure 1 for details). Sample 9 is a block (20 mm x 25 mm) whose base height is approximately 10.57 mm above a sub-plate with sub-regions 9B to 9E each increasing in height by one layer (40 μm). An integrated coordinate system is 'burned' on the sample using the laser (no additional powder) to enable the location of specific regions on the different measurement systems. The build was performed on a 127 mm x 127 mm x 12.5 mm sub-plate, which was bolted to the center of the LPBF machine's build plate. Figure 1 also indicates the locations of the sample and sub regions with respect to the sub-plate and machine argon gas delivery source.

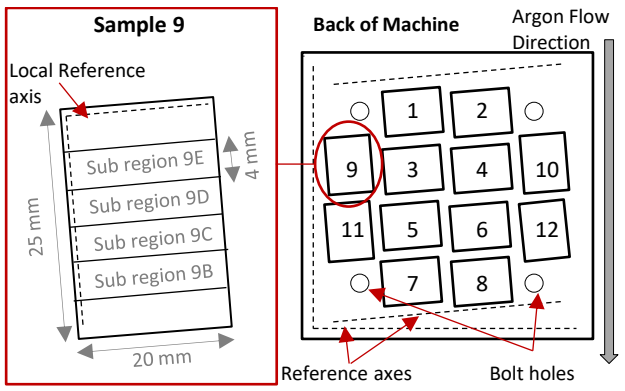

Figure 1. Schematic (top-down view) of sample 9 (left) and build layout of the 127 mm x 127 mm subplate (right).

Measurements of the first set of samples showed unexpected films and particulates, which might have been a by-product of the wire electrical discharge machining (EDM) removal of samples from the build plate, or handling protocols [5]. Thus, for the second set, loose powder was removed with care to minimize interaction with the sample surfaces and the entire sub-plate was double bagged until cleaning.

Cleaning was performed with the sub-plate face down in two room temperature ultrasonic baths, first in acetone and then in high purity ethanol. Initial coherence scanning interferometer

(CSI) measurements were performed before any machining to remove samples from the build plate.

The surface metrology results presented here were obtained using a Zygo NexView CSI with a 50x (0.55 NA) Mirau objective (spatial sampling 0.17 µm/pixel with 4x oversampling to minimize data drop-out) [6]. Features of interest (FoI) have lateral scales from hundreds of micrometers to below the diffraction limit. The Sparrow criterion indicates a limiting lateral resolution of 0.52 µm. Smaller discrete features may be identified [7] although the amplitude reported is not reliable. To reach the longer spatial wavelength of interest, stitching algorithms native to the Zygo MX software are used [8].

Intensity images in the CSI are in focus at every pixel on rough surfaces. The modulation intensity mode provides high contrast surface images that facilitate identification of FoI for detailed evaluations of height maps and, using the developed coordinate systems, locating FoI in other measurement tools.

Scanning electron microscope (SEM) images were acquired on a ZEISS GEMINI SEM 450, Secondary Electron (SE) and In-lens SE-detectors. Energy Dispersive Spectroscopy (EDS) was performed at 5kV with an Oxford UltimMax 100 mm^2 large area Analytical Silicon Drift Detector (SDD). To facilitate these measurements, the sub-plate was sectioned using a bandsaw with no cooling fluids to prevent contamination. To prevent damage to the sample, sectioning was performed through the sub-plate to separate sample 9 from the rest of the build. Sample 9 was then re-cleaned ultrasonically using ethanol for 8 minutes before packaging and shipping to the Zeiss facility for measurement.

3. Results

In investigating the height and intensity data from the CSI system, the expected chevron patterns are more subtle in this sample because build conditions led to large length-to-width melt pool ratios such as those seen in [4]. Several other textures and fine scale features were present in addition to flow lines and chevron patterns. This section will detail the various structures found on the sample surface and Figure 2 depicts the relevant size scales observed.

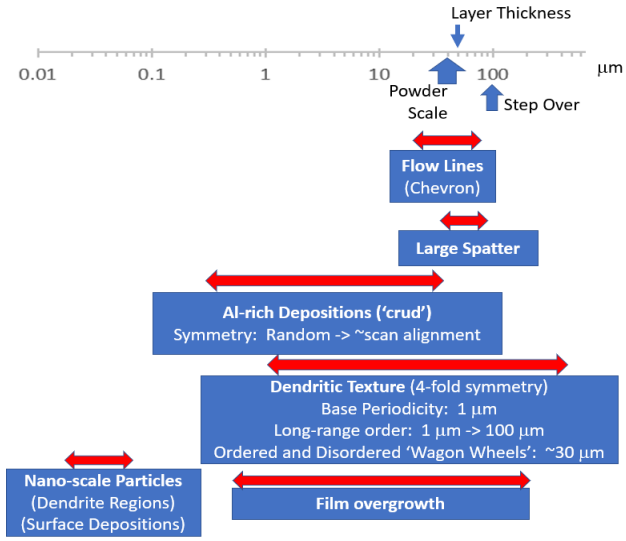

Figure 2. Graphical representation of size scales observed for features of interest.

An intensity image from the Zygo system, which captures many of the FoIs, and an SEM image of the same area are shown in Figure 3 and Figure 4, respectively.

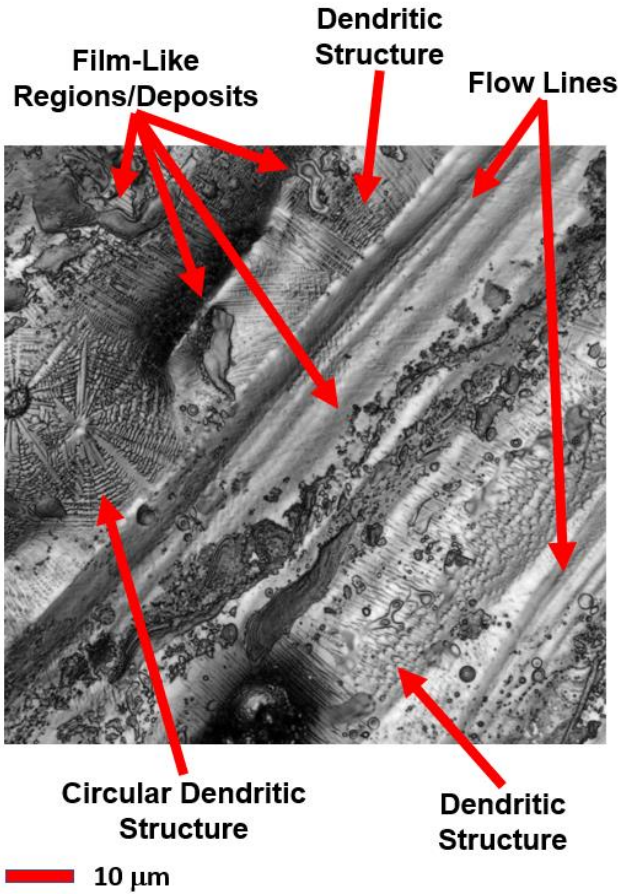

Figure 3. Intensity image from the Zygo Nexview CSI with various structures identified. Direction of laser path is ≈45° through the image.

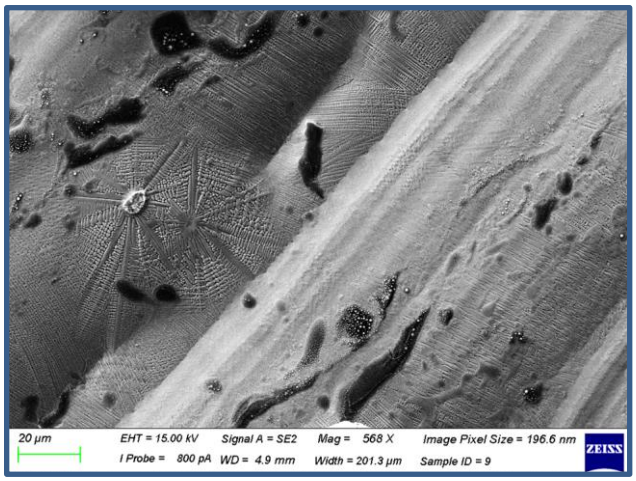

Figure 4. SEM image of approximately the same region as Figure 3.

3.1. Film-like Regions and Deposits

Across the surface there are regions of a film-like structure that appear to obscure other features. These structures were previously thought to be contamination from the wire electrical discharge machining (EDM) but are present without subjecting the part to that process thus nullifying that hypothesis. Size scales of these regions are on the order of below 1 µm to tens of micrometers. They are irregular in shape but tend to cluster somewhat parallel to the direction of the laser path. These are seen labeled in Figure 3 and as dark regions in Figure 4. Figure 5 presents results of an elemental analysis of a similar region via EDS. From the elemental analysis, the deposit has very high aluminum and oxygen content. For reference, the material

specification for IN625 requires aluminum to be less than 0.4% with no oxygen specified. Additionally, the LPBF process is performed in an inert argon environment. It is hypothesized that the aluminum content is vaporized in the fusion process and subsequently re-deposited on the surface, with oxygen being a contamination pickup from powder recycling/storage/reuse [9] or atmospheric oxidation of an aluminum film. Additional analysis is ongoing.

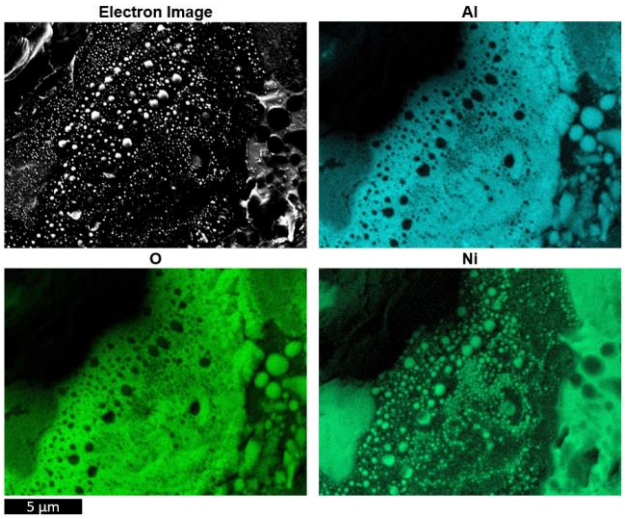

Figure 5. Elemental window integral maps from EDS of a film-like region. Only aluminum, oxygen, and nickel maps are shown for brevity.

3.2. Dendritic Structures

Dendritic structures are another common feature seen on the surface and have varying characteristics. Dendritic structures are expected for IN625 [10]. Common among all the dendritic structures is a base periodicity of ≈1 µm and long-range order from 1 µm to ≈100 µm. Some of the dendritic structures appear in a near circular shape with rotational symmetry and primary dendrites forming a line between the edge and the center of the structure with orthogonal secondary dendrites. The pattern resembles a "wagon wheel" and is observed to have diameters in the tens of micrometers range with either a small depression (100's nm scale) or particle (10's µm scale) at the center, suggesting these structures are related to particle impacts on the surface (i.e., either ejecta remelting part of the surface or particles solidifying a portion of the melt pool on contact). An example, seen in an SEM image, is shown in Figure 6.

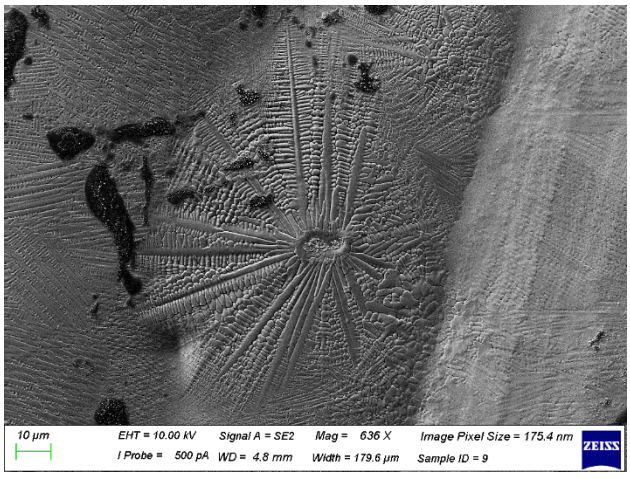

Figure 6. A circular dendritic microstructure.

Height measurement of one such structure, with a cylinder form removal and digital Gaussian high-pass filter of 30 µm, shows a peak to valley height profile of approximately 1 µm and width between 10 µm and 20 µm.

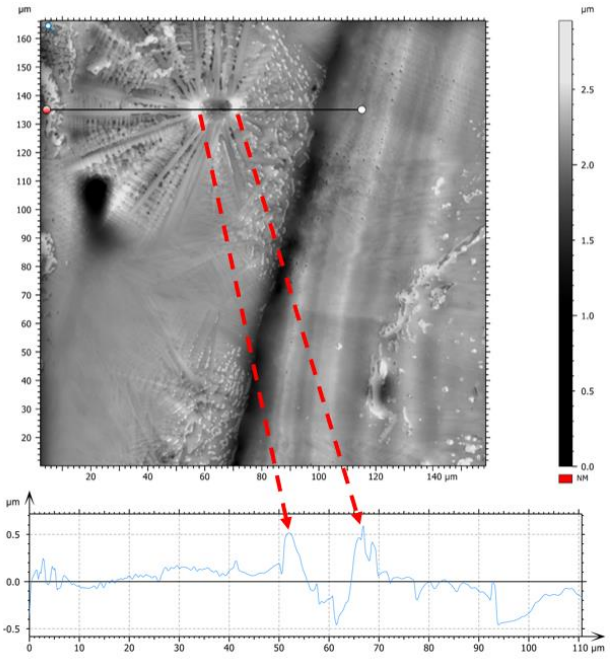

Figure 7. Height map of circular dendritic structure

In some instances, circular or near circular dendritic structures were found with a disordered appearance (i.e., no clear center to boundary line for primary dendrites) as shown in Figure 8. Currently, it is not clear what conditions would be necessary to create such a structure.

Much more common than the "wagon wheel" and "disordered" dendritic structures, however, are the dendritic structures without the rotational symmetry. These regions can be seen labeled in Figure 3 and cover large length scales (i.e., tens to hundreds of micrometers) and, as previously shown, are an expected condition of as-built AM IN625 [10].

Figure 8. SEM image of the "disordered" dendritic structure.

3.3. Nanoscale "Particles"

Closer inspection of the surface has shown nanoscale features in both the aluminum rich deposits and across dendritic structures (e.g., Figure 9). It is hypothesized that these are Laves phase structures, though additional analysis is required to confirm.

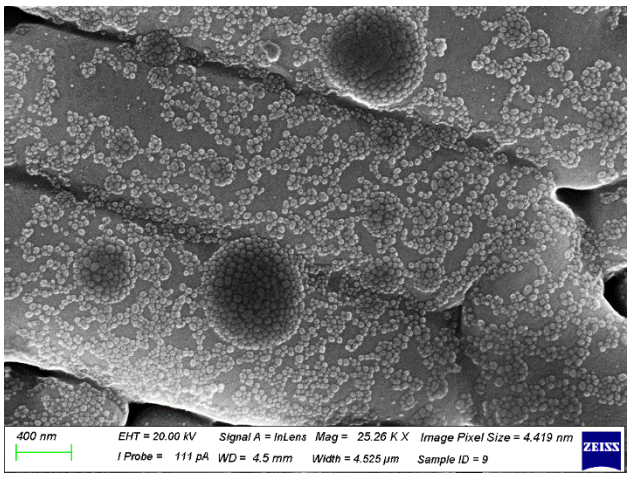

Figure 9. SEM image of nanoscale "particles" seen on a dendritic structure

4. Conclusions and further work

Often, AM literature focuses on surface structures in the 1 µm and greater regime, as smaller features challenge the capabilities of conventional geometrical metrology equipment. However, this study has found several features of interest down to even tens of nanometers. These features, which are well summarized in Figure 2, are more prevalent than the expected flow lines and chevron patterns commonly seen. In this work, height data and intensity images from CSI measurements along with SEM and EDS measurements were used to investigate and identify these features. Measurements were carefully aligned using part coordinate systems printed in the LPBF machine during builds, allowing for detailed analysis of multiple forms of data simultaneously.

Film-like structures on the surface were identified to have high concentrations of aluminum and oxygen. These are hypothesized to be vaporized aluminum from the fusion process and oxygen exposure from powder storage in an air environment prior to reuse. Regardless, these indicate local chemistry deviation from required material specifications.

Dendritic microstructure with a base short-range order of ≈1 µm were seen in SEM images, and careful alignment of data sources allowed for confirmation of their signature in CSI intensity images. Ordered dendritic structures are most common, which are expected for as-built AM IN625. "Wagon wheel" like structures with radial primary dendrites and orthogonal secondary dendrites are present and hypothesized to nucleate from particle or ejecta impacts. Some of the dendritic structures are disordered and lack the radial primary dendrites. Finally, nanometer-scale particles are present on the surface over dendritic structures and the film-like regions. We suspect these are Laves phase structures, but additional testing is required to confirm.

Future work will include determining the quantity of various structures. This will give insight into situations that create greater or fewer instances of the various structures. Powder characterization is being performed to help determine the source of the oxygen and aluminum concentrations, and further metallurgical testing is planned. These investigations will help relate the surface structures to the aspects of the process that created them and aid in the development of process-structure-property relationships.

Acknowledgements

This work was supported in part by Zeiss and in part by the Center for Precision Metrology at UNC Charlotte. The authors would also like to thank Jared Tarr at the National Institute of Standards and Technology for his assistance with the fabrication of test samples and Greg Caskey for his assistance with measurements on the Nexview system.

Disclaimer

Certain commercial entities, equipment, or materials may be identified in this document to describe an experimental procedure or concept adequately. Such identification is not intended to imply recommendation or endorsement by the National Institute of Standards and Technology, nor is it intended to imply that the entities, materials, or equipment are necessarily the best available for the purpose.

References

[1] N. Senin, A. Thompson, R.K. Leach, Characterisation of the topography of metal additive surface features with different measurement technologies, Meas. Sci. Technol. 28 (2017) 095003.

[2] R.K. Leach, D. Bourell, S. Carmignato, A. Donmez, N. Senin, W. Dewulf, Geometrical metrology for metal additive manufacturing, CIRP Ann. 68 (2019) 677–700.

[3] Z.C. Reese, J.C. Fox, J. Taylor, C. Evans, Evolution of Cooling Length in Parts Created Through Laser Powder Bed Fusion Additive Manufacturing, in: Proc. 2018 ASPE Euspen Summer Top. Meet. - Adv. Precis. Addit. Manuf., Berkeley, CA, 2018: pp. 183–188. https://www.nist.gov/publications/evolution-cooling-length-parts-created-through-laser-powder-bed-fusion-additive (accessed January 7, 2020).

[4] R.E. Ricker, J.C. Heigel, B.M. Lane, I. Zhirnov, L.E. Levine, Topographic Measurement of Individual Laser Tracks in Alloy 625 Bare Plates, Integrating Mater. Manuf. Innov. 8 (2019). https://www.ncbi.nlm.nih.gov/pmc/articles/PMC7537414/ (accessed June 18, 2021).

[5] Z.C. Reese, J.C. Fox, F.H. Kim, J. Taylor, C. Evans, Effect of Subsurface Defects on the Surface Topography of Additive Manufactured Components, in: Proc. 2018 ASPE Euspen Summer Top. Meet. - Adv. Precis. Addit. Manuf., Berkeley, CA, 2018: pp. 127–131. https://www.nist.gov/publications/effect-subsurface-defects-surface-topography-additive-manufactured-components (accessed January 7, 2020).

[6] C. Gomez, R. Su, A. Thompson, J. DiSciacca, S. Lawes, R.K. Leach, Optimization of surface measurement for metal additive manufacturing using coherence scanning interferometry, Opt. Eng. 56 (2017) 111714.

[7] The Meaning and Measure of Lateral Resolution for Surface Profiling Interferometers, (n.d.). https://www.osa-opn.org/home/articles/volume_23/issue_4/departments/optical_engineering/optical_engineering/ (accessed June 21, 2021).

[8] Mx Software, v8.0.0.26, Zygo Corporation, Middlefield, CT., 2019.

[9] N. Emminghaus, C. Hoff, J. Hermsdorf, S. Kaierle, Residual oxygen content and powder recycling: Effects on surface roughness and porosity of additively manufactured Ti-6Al-4V, Addit. Manuf. 46 (2021) 102093.

[10] F. Zhang, L.E. Levine, A.J. Allen, M.R. Stoudt, G. Lindwall, E.A. Lass, M.E. Williams, Y. Idell, C.E. Campbell, Effect of heat treatment on the microstructural evolution of a nickel-based superalloy additive-manufactured by laser powder bed fusion, Acta Mater. 152 (2018) 200–214.